Supplemental Data

Self-associated molecular patterns mediate cancer immune evasion by engagement of Siglec receptors on T cells

Michal A. Stanczak, Shoib S. Siddiqui, Marcel P. Trefny, Daniela S. Thommen, Kayluz Frias Boligan, Stephan von Gunten, Alexandar Tzankov, Lothar Tietze, Didier Lardinois, Viola Heinzelmann-Schwarz, Michael von Bergwelt-Baidon, Wu Zhang, Heinz-Josef Lenz, Younghun Han, Christopher I. Amos, Mohammedyaseen Syedbasha, Adrian Egli, Frank Stenner, Daniel E. Speiser, Ajit Varki, Alfred Zippelius and Heinz Läubli

Supplemental material and methods

Antibodies.

The following antibodies were used for Siglec-9 staining. The blocking clone 191240 was used for flow cytometry staining and blocking experiments (R&D Systems). In some experiments, also the non-blocking monoclonal antibody clone E10-286 was used (BD Biosciences). Fab fragments of the 191240 anti-Siglec-9 antibody were generated using the Pierce Fab Micro Preparation kit (Thermo Scientific). The following antibodies were used for staining of human cells in multicolor flow cytometry analysis: Anti-CD4-BV711 (clone SK3), anti-IFNγ-BV421 (4S.B3), anti-PD1-PE-Cy7 (EH12.1), anti-BTLA-PE (J168-540), anti-active caspase 3-PE (C92-605) were purchased from BD; anti-CD45-PerCP Cy 5.5 (2D1), anti-CD3-APC eF780 (SK7), anti-4-1BB-FITC (4B4), anti-CD25-PE (CD25-4E3), anti-IL-2-PE (MQ1-17H12), anti-TNFα-APC (MAb11), anti-Perforin-FITC (dG9), anti-LAG-3-FITC (3DS223H), anti-TIGIT-PE (MBSA43) were purchased from eBioscience; anti-CD8-BV605 (SK1), anti-TIM-3-BV421 (F38-2E2), anti-CD160-eF660 (BY55), anti-CD25-BV421 (BC96), anti-Foxp3-AF647 (259D) were purchased from Biolegend; anti-EPCAM-FITC (HEA-125) was purchased from Miltenyi. For flow cytometry staining of murine cells, the following antibodies were used: anti-CD25 (PC61.5), anti-CD45 (A20), anti-CD3 (145-2C11), anti-CD8a (53-6.7), anti-CD11b (M1/70), anti-CD11c (N418), anti-PD-1 (29F.1A12), anti-Tbet (O4-46) and anti-TIM-3 (RMT3-23). For Mo-MDSC and PMN-MDSC determination, anti-CD11b (M1/70), anti-Ly6C (HK1.4), and anti-Ly6G (1A8) antibodies were used. All FACS antibodies for analysis of murine cells were purchased from Biolegend or BD Biosciences.

Siglec-Fc production.

Siglec-Fcs were produced using previously described Siglec-Fc expression plasmids. Briefly, the three N-terminal domains of Siglec-9 were cloned into a human-Fc fusion vector and mutants generated by site-directed mutagenesis. Plasmids were transfected using polyethylenimine (PEI) into 293T HEK cells, cultured in serum free expression medium and supernatants harvested after 72h. Siglec-Fcs were purified using protein A beads and desialylated on column using *Vibrio Cholerae* neuraminidase (VCN) to minimize *cis*-interactions. After elution and concentration by ultracentrifugation, protein concentration was

determined by BCA measurement and functionality assessed by SDS-PAGE and FACS-staining of tumor cell lines.

Histology and immunofluorescence.

For Siglec staining, frozen sections of tumor samples were prepared with a cryostat. Siglec-9 was stained with a monoclonal antibody (R&D Systems) and detected with a secondary, biotinylated anti-mouse IgG and subsequent incubation with streptavidin-HRP. Mouse tissues and immunofluorescence costaining was also performed on frozen sections. For immunofluorescence, primary antibodies were detected with secondary Cy5 or Alex488-coupled antibodies.

Multiplex cytokine measurements.

Siglec-9 positive and negative TILs were sorted from frozen primary NSCLC samples by flow cytometry as described above. Flat bottom 96 well plates were coated over night with anti-CD3 antibody (0.5 µg/ml), T cells plated at 50 000 cells/well and soluble anti-CD28 antibody added (1 µg/ml). After polyclonal stimulation, supernatants were collected, spun down and kept at -80 °C. Inflammatory chemokines and cytokines were measured by a flow cytometry based bead assay (CBA) that allows measurement of 13 inflammatory chemokines or cytokines simultaneously (both from BioLegend). Binding of cytokines to the beads was measured on a Fortessa LSR II flow cytometer (BD Biosciences).

GNE-deficient tumor cells in vivo*.*

All mouse experiments were approved by the local ethical committee (Ethical Committee of Basel Stadt). Wildtype mice were bought from Janvier Labs or bred in the animal facility of the Department of Biomedicine at the University of Basel, Switzerland. MC38 were provided by Mark Smyth (Peter MacCallum Cancer Centre, Melbourne, AU), and EMT6 were bought from ATCC. For the transplantable syngeneic MC38 or EMT6 tumor models, 500'000 tumor cells were injected subcutaneously into the right thoracic flank of 8 to 12-week-old female C57BL/6 or BALB/c mice respectively. Perpendicular tumor diameters were measured by caliper, and tumor volume calculated according to the following formula: tumor volume (mm^3) = $d^2*D/2$, where D and d are the longest and shortest diameters of the tumor (in millimeters),

respectively. GNE-deficient MC38 or EMT6 cells were generated as described above. Tumor growth was measured three times a week and compared to the growth of WT cell lines. Cell growth in vitro was not different between GNE-KO cells and WT counterparts. Animals whose tumors had reached 1200 mm^3 were euthanized, and animals having developed ulcerations removed from the experiment. Proliferation of GNE-KO lines were done by counting with a hemocytometer or a MTT assay. Viability was tested by incubating with trypan blue.

Supplemental Figures and Tables

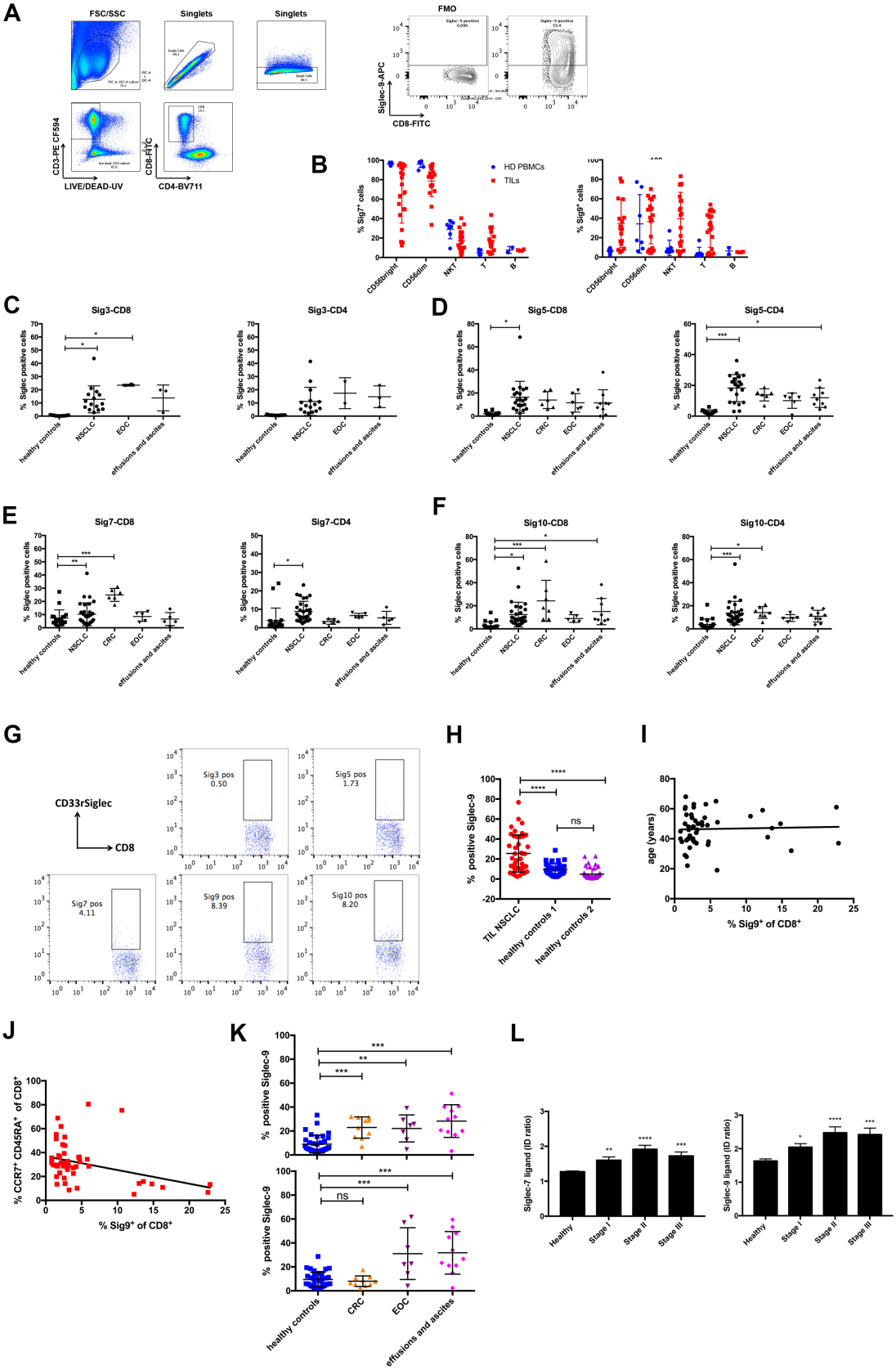

Supplemental Figure 1 Upregulation of CD33-related Siglecs on TILs.

(**A**) Demonstration of gating for Siglec-9 expression on CD8+ TILs from primary NSCLC samples (FMO, fluorescence minus one control). (**B**) Percent of cells with expression of Siglec-7 (left panel) or Siglec-9 (right panel) on myeloid cells, NK cells or B cells in NSCLC tumor samples by flow cytometry (HD PBMCs *n*=6, TILs *n*= 20). NK cells were determined as $CD45^+$ $CD56^+$ $CD3^-$, NKT cells as $CD45^+$ $CD56^+$ $CD3^+$, myeloid cells as $CD45^+$ $CD11b^+$ cells. Also, a comparison with $CD20^+$ B cells and $CD3^+$ T cells was done. (**C**) Upregulation of inhibitory CD33 (Siglec-3) on $CD8^+$ and $CD4^+$ T cells in the PBMCs from healthy controls, primary NSCLC, CRC, EOC samples or in ascites (mainly colorectal cancers) and pleural effusions (NSCLC samples, *n*=3-15). (**D**) Percentage of $CD8^+$ and $CD4^+$ T cells expressing Siglec-5 from healthy donors and cancer patients determined by flow cytometry (*n*=5-25). (**E**) Expression of Siglec-7 on PBMCs and TILs (*n*=5-25). (**F**) Expression of Siglec-10 on PBMCs and TILs (*n*=5-25). (**G**) CD33-related Siglec expression on $CD8^+$ human splenocytes from a patient that underwent splenectomy due to an accident. (**H**) Additional staining of Siglec-9 on $CD8^+$ peripheral T cells in an additional cohort of healthy controls (group 2, *n*=49) and comparison with previous control cohort (group 1, n=36) and TILs from NSCLC samples (*n*=41, same samples as in Figure 1C). (**I**) Correlation of the number of $Sig9^+$ $CD8^+$ T cells in the peripheral blood of healthy donors with age (*P*=0.8 by linear regression analysis). (**J**) Correlation of the number of $Sig9^+$ $CD8^+$ T cells in the peripheral blood of healthy donors with the number of $CD45RA^+$ $CCR7^+$ $CD8^+$ naïve T cells (*P*=0.017 by linear regression analysis). (**K**) Siglec-9 expression of $CD4^+$ (upper panel) and $CD8^+$ (lower panel) TILs from patients with CRC, EOC and pleural effusions (PBMCs *n*=36, CRC *n*=10, EOC *n*=7, pleural effusion *n*=11). (**L**) Detection of Siglec-7 (upper panel) or Siglec-9 (lower panel) ligands on an NSCLC tissue microarray (n=40, mean±s.e.m). Siglec-7 or Siglec-9 ligands were upregulated in all NSCLC stages. Statistical analysis was performed by Student's t test for 2 conditions and 1-way-ANOVA for multiple conditions. **P*<0.05, ***P*<0.01, ****P*<0.001. Data presented as mean±s.d. if not otherwise stated.

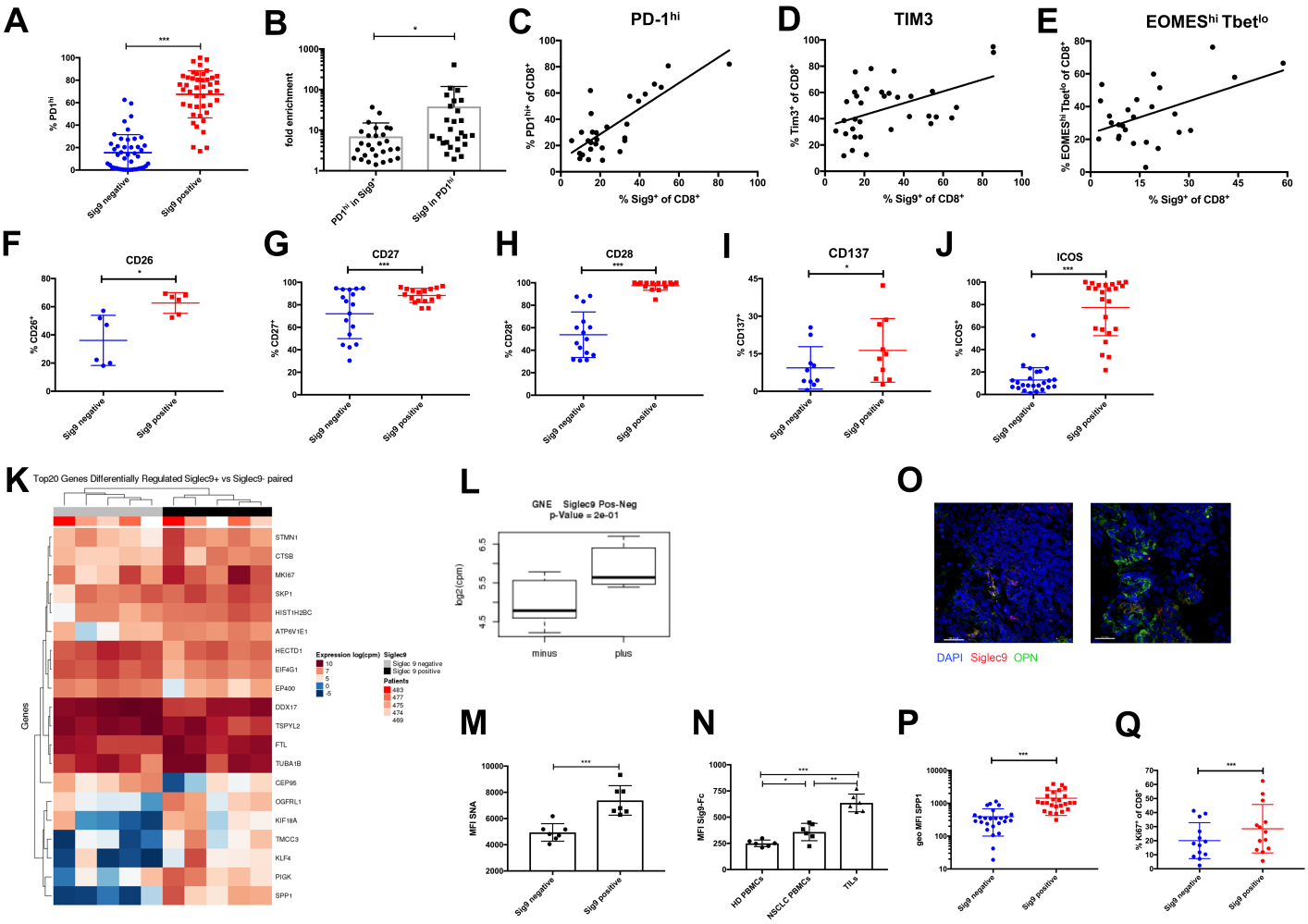

Supplemental Figure 2 Characterization of Sig9^{+} CD8^{+} TILs.

(**A**) Percentage of PD-1 high expressing cell determined by FACS on Sig9^{+} CD8^{+} TILs and Sig9^{-} CD8^{+} TILs in NSCLC tumor samples (*n*=44). (**B**) Fold enrichment of PD-1^{hi} in Sig9^{+} CD8^{+} TIL population or Sig9^{+} in PD-1^{hi} CD8^{+} TIL population. This shows that Sig9^{+} CD8^{+} TILs are a subpopulation of the PD-1^{hi} CD8^{+} TIL population. (**C**) Correlation of Sig9^{+} with PD-1^{hi} percentage of CD8^{+} TILs in NSCLC tumor sample (*P*<0.001, by linear correlation analysis). (**D**) Correlation of Sig9^{+} with TIM-3^{+} percentage of CD8^{+} TILs in NSCLC tumor sample (*P*=0.0042, by linear correlation analysis). (**E**) Correlation of EOMES^{hi} Tbet^{lo} cells with Sig9^{+} CD8^{+} TILs (*P*=0.095, by linear correlation analysis). (**F-J**) Expression of costimulatory receptors CD26 (F, *n*=6), CD27 (G, *n*=17), CD28 (H, *n*=15), CD137 (I, *n*=10) and ICOS (J, *n*=23) on Sig9^{-} and Sig9^{+} CD8^{+} TILs from NSCLC samples. (**K**) Heatmap of expression of top 20 differentially expressed genes determined by RNA sequencing of sorted Sig9^{+} CD8^{+} TILs and compared to

Sig9$^-$ CD8$^+$ TILs (*n*=5 samples were sorted). (**L**) Expression analysis of mRNA levels by RNA sequencing of GNE in Sig9$^+$ and Sig9$^-$ TILs (5 samples). (**M**) Staining Sig9$^-$ CD8$^+$ or Sig9$^+$ CD8$^+$ TILs by flow cytometry with SNA (*n*=6-7). (**N**) Binding of Siglec-9-Fc to CD8$^+$ T cells from healthy donor (HD) PBMCs, PBMCs from NSCLC patients or TILs from NSCLC patients (*n*=6-7). (**O**) Fluorescence staining of osteopontin (OPN) and Siglec-9 on primary NSCLC tumor samples (bars, 30μm). In the left panel, mononuclear OPN$^+$ Sig9$^+$ cells T cells can be seen. On the right panel (different sample), tumor cells OPN positive and OPN$^+$ Sig9$^+$ double positive cells have macrophage morphology. (**P**) Intracellular expression of SPP1 (osteopontin) in Sig9$^-$ CD8$^+$ TILs or Sig9$^+$ CD8$^+$ TILs from primary NSCLC samples measured by flow cytometry (*n*=25). (**Q**) Expression of Ki67 (MKI67) in Sig9$^-$ CD8$^+$ TILs or Sig9$^+$ CD8$^+$ TILs by flow cytometry (*n*=12). **P*<0.05, ****P*<0.001. Data presented as mean±s.d.

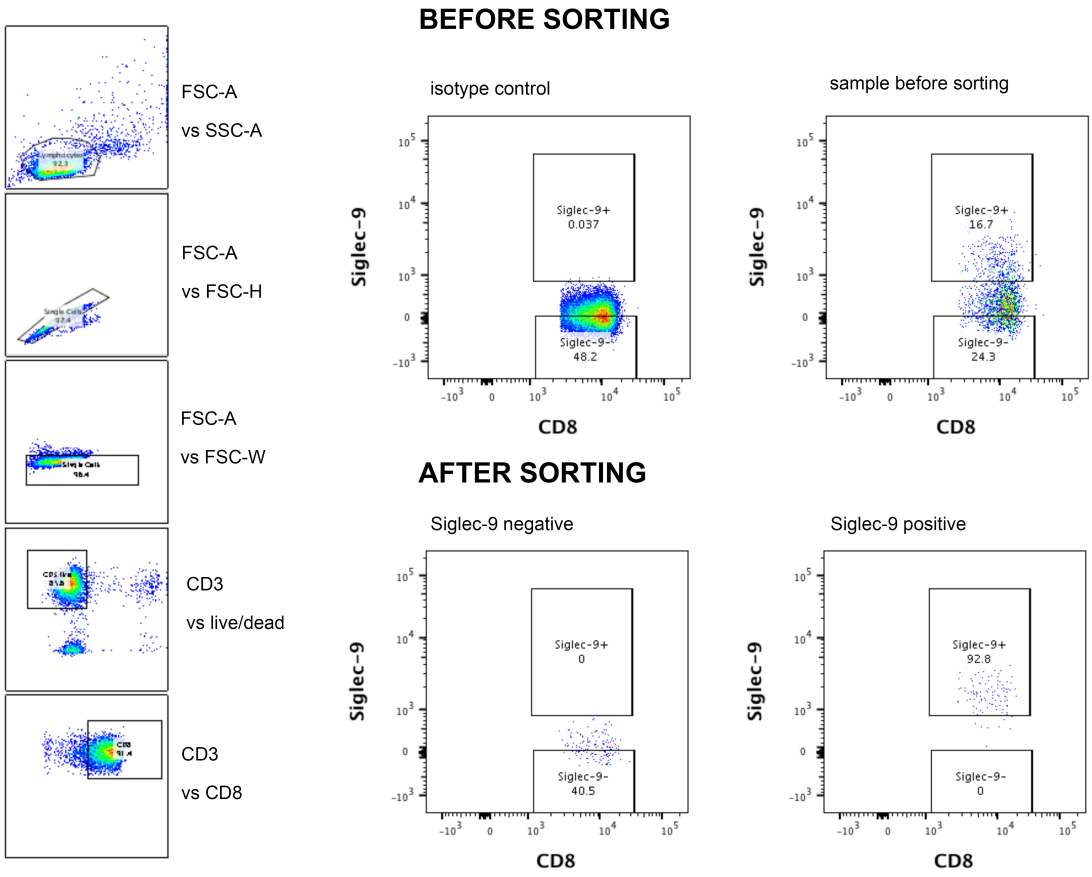

Supplemental Figure 3 Gating strategy for sorting of Sig9^{+} CD8^{+} TILs from NSCLC samples.

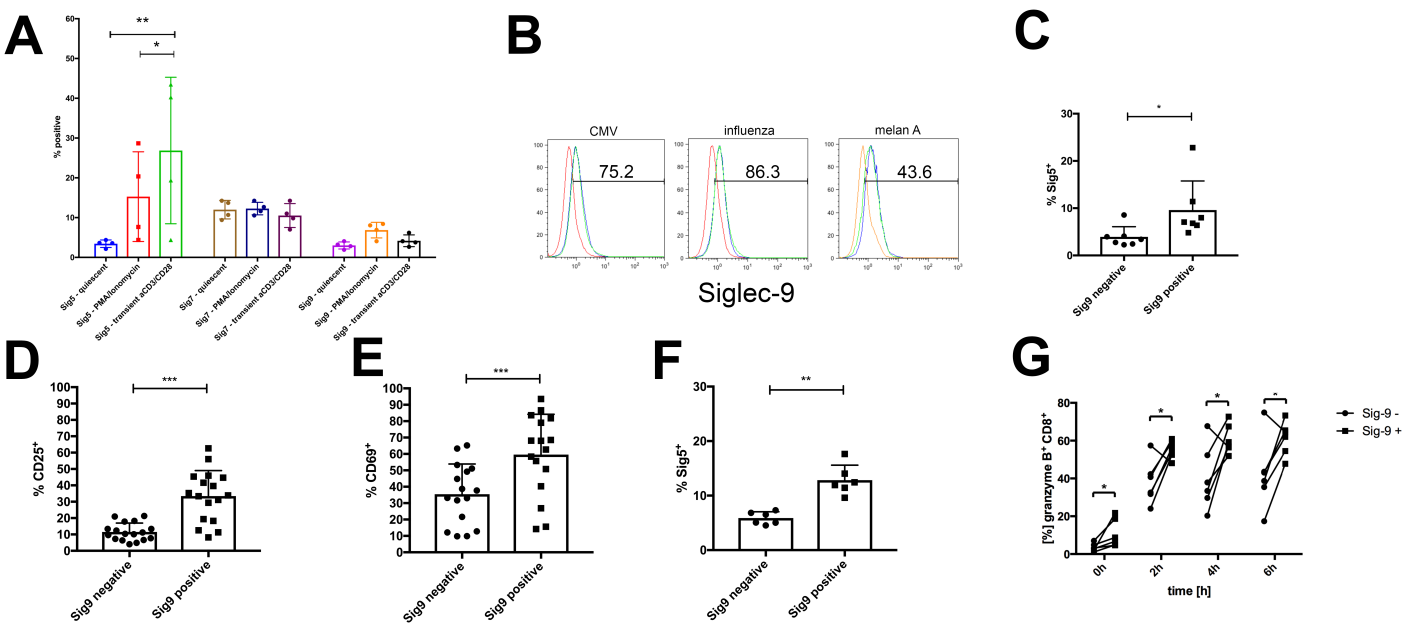

Supplemental Figure 4 Functional characterization of Sig9$^+$ CD8$^+$ TILs.

(**A**) Upregulation of Siglec-5, Siglec-7, Siglec-9 on activated CD8$^+$ T cells from healthy donors. Activation was obtained by short-time stimulation with anti-CD3 and anti-CD28 antibodies or PMA/Ionomycin (*n*=4). (**B**) Upregulation of Siglec-9 on CD8$^+$ T cell clones stimulated with a specific antigen (CMV, influenza and melan A) measured by flow cytometry. Representative images of T cell clones. (**C**) Siglec-5 is used as an additional activation marker on TILs sorted from NSCLC samples according to Siglec-9 expression (*n*=7). (**D**) Upregulation of the activation marker CD25 on the surface of polyclonally stimulated (anti-CD3/28 antibodies) Sig9$^+$ and Sig9$^-$ CD8$^+$ T cells in the peripheral blood of healthy donors. The expression was determined by flow cytometry (*n*=17 different healthy donors). (**E**) CD69 was determined on Sig9$^+$ and Sig9$^-$ CD8$^+$ T cells in the peripheral blood of healthy donors after polyclonal stimulation (*n*=16). (**F**) The newly identified activation marker Siglec-5 was determined on Sig9$^+$ and Sig9$^-$ CD8$^+$ T cells in the peripheral blood of healthy donors after polyclonal stimulation (*n*=6). (**G**) Upregulation of intracellular granzymeB in Sig9$^+$ and Sig9$^-$ CD8$^+$ TILs from NSCLC patients after different durations of stimulation with anti-CD3 and anti-CD28 antibodies (*n*=6). **P*<0.05, ***P*<0.01, ****P*<0.001. Data presented as mean±s.d.

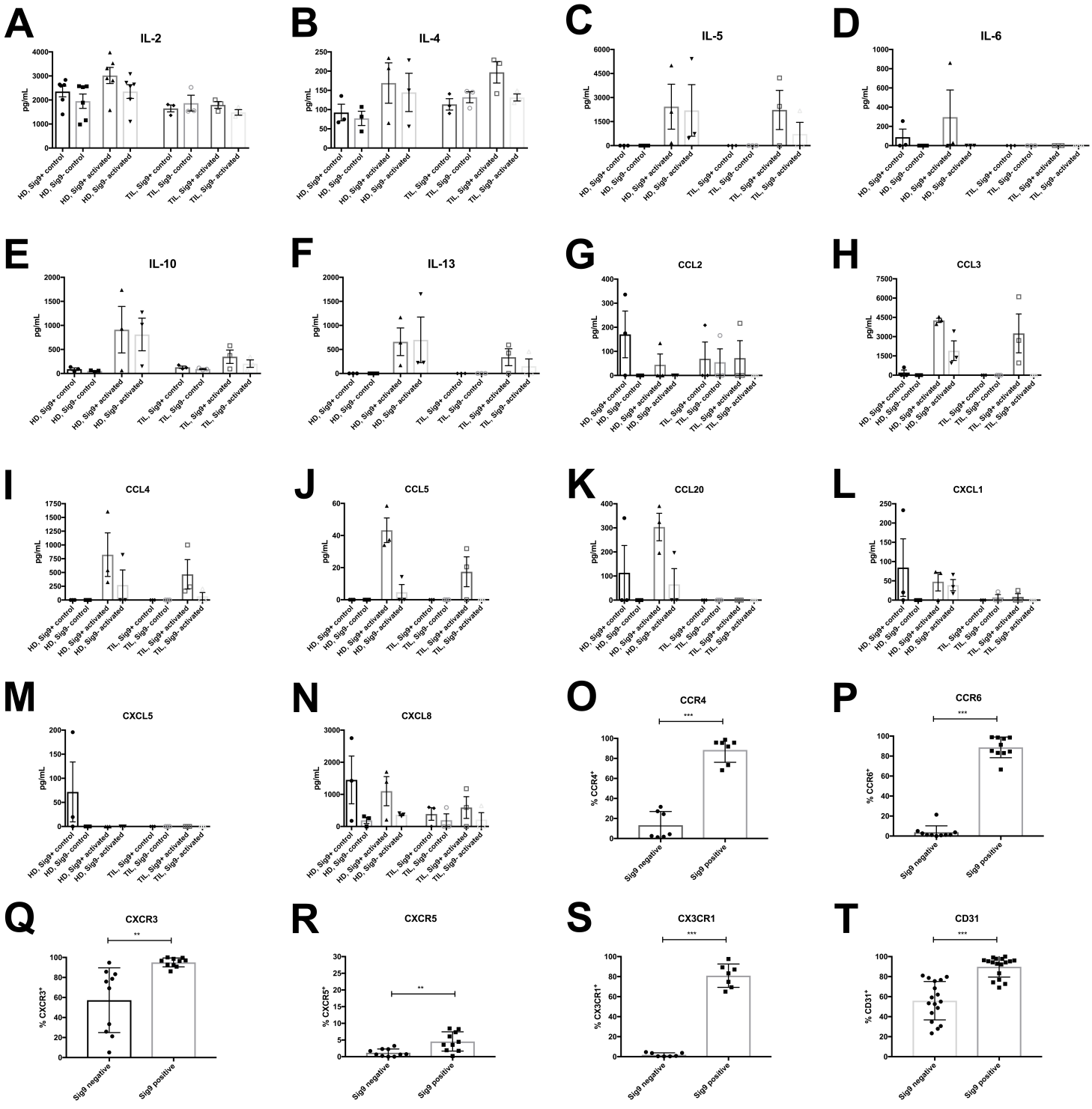
A
IL-2
B
IL-4
C
IL-5
D
IL-6
E
IL-10
F
IL-13
G
CCL2
H
CCL3
I
CCL4
J
CCL5
K
CCL20
L
CXCL1
M
CXCL5
N
CXCL8
O
CCR4
P
CCR6
Q
CXCR3
R
CXCR5
S
CX3CR1
T
CD31
pg/mL
% CCR4+
% CCR6+
% CXCR3+
% CXCR5+
% CX3CR1+
% CD31+
HD, Sig9+ control
HD, Sig9- control
HD, Sig9+ activated
HD, Sig9- activated
TIL, Sig9+ control
TIL, Sig9- control
TIL, Sig9+ activated
TIL, Sig9- activated
Sig9 negative
Sig9 positive

Supplemental Figure 5 Expression of cytokines of Sig9$^+$ CD8$^+$ TILs.

(**A-F**) Determination of cytokines in the supernatant of sorted Sig9$^+$ and Sig9$^-$ CD8$^+$ TILs from NSCLC patients by a multiplex bead assay (Biolegend). The secretion was also compared to Sig9$^+$ and Sig9$^-$ CD8$^+$ T cells sorted from PBMCs of healthy donors (*n*=3-7). (**G-N**) Determination of chemokines in the supernatant of sorted Sig9$^+$ and Sig9$^-$ CD8$^+$ TILs from NSCLC patients and compared to Sig9$^+$ and Sig9$^-$ CD8$^+$ T cells sorted from PBMCs of healthy donors (*n*=3). (**O-T**) Frequency in percent of chemokine receptor expression on Sig9$^-$ CD8$^+$ TILs or Sig9$^+$ CD8$^+$ TILs in primary NSCLC samples determined by flow cytometry (*n*=10). **P*<0.05, ***P*<0.01, ****P*<0.001. Data presented as mean±s.d.

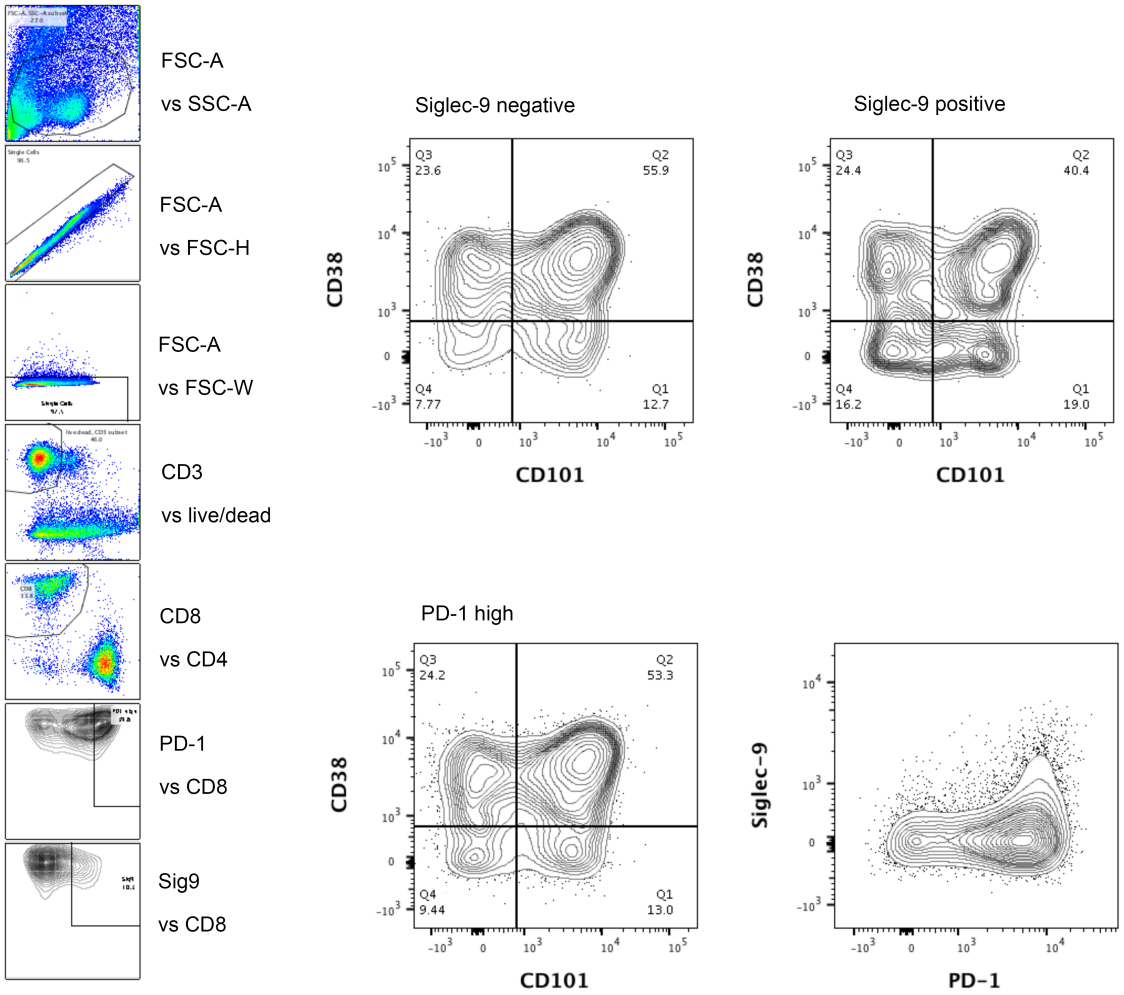

Supplemental Figure 6 Gating strategy for the detection of CD101 and CD38 on Sig9^{+} CD8^{+} TILs from NSCLC samples.

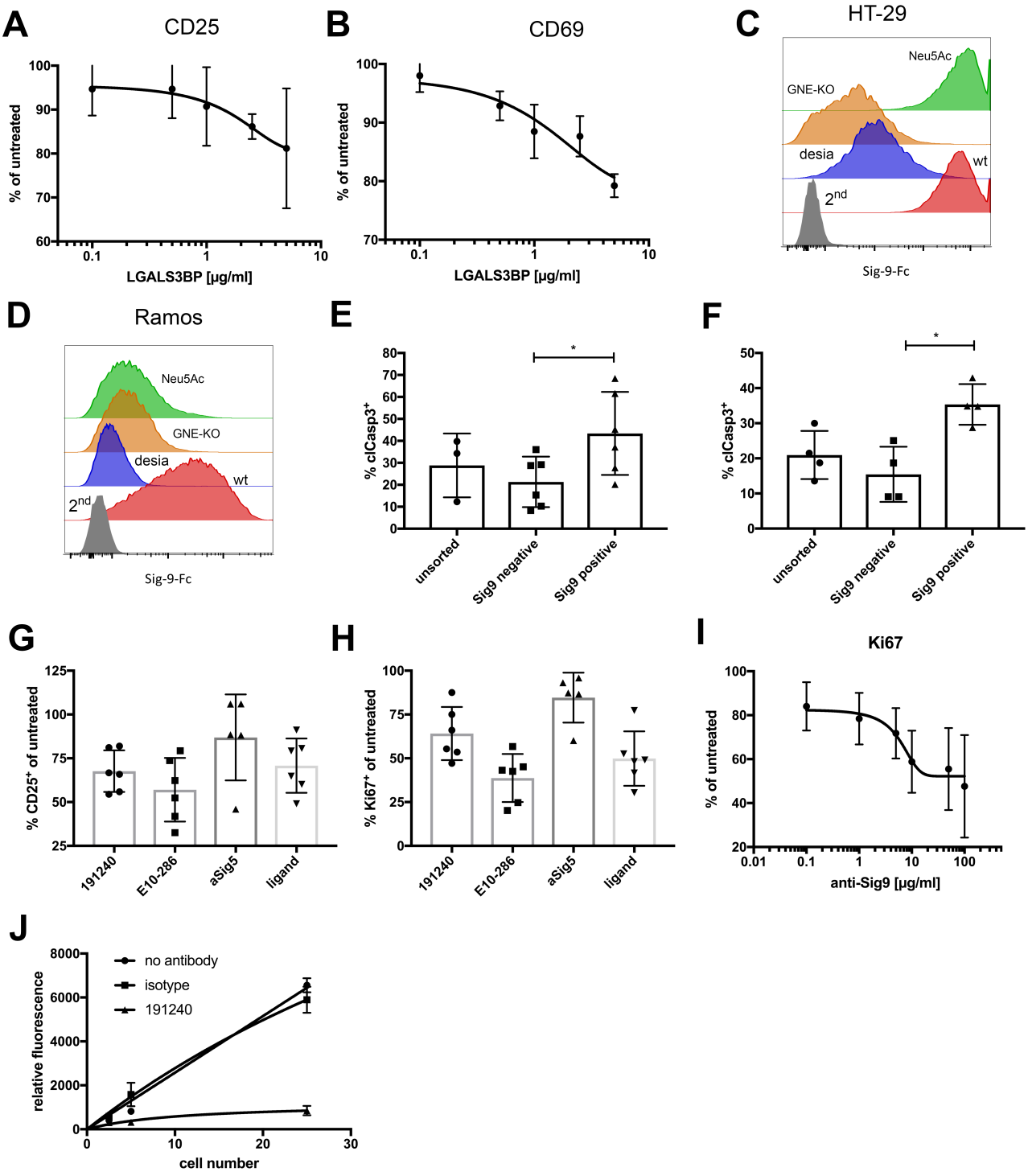

Supplemental Figure 7 Siglec-sialoglycan-SAMP interactions influence T cell effector function.

(**A**) Expression of CD25 analyzed by flow cytometry on the surface of polyclonal stimulated CD8$^+$ T cells in the presence of the Siglec ligand LGALS3BP over a dose range (*n*=3

independent donors). (**B**) Expression of the activation marker CD69 polyclonal stimulated $CD8^+$ T cells in the presence of the Siglec ligand LGALS3BP (*n*=3 independent donors). (**C**) Binding of Siglec-9-Fc to different HT-29 cells. Wildtype cells (WT) were compared to desialylated (desia), GNE-deficient (GNE-KO) and GNE-deficient with excess of sialic acid (Neu5Ac) in the medium cells. (**D**) Binding to different $CD19^+$ Ramos cells. Wildtype cells (WT) were compared to desialylated (desia), GNE-deficient (GNE-KO) and GNE-deficient with excess of sialic acid (Neu5Ac) in the medium cells. (**E**) Induction of apoptosis measured by cleaved caspase 3 (clCasp3) in A549 cells incubated with unsorted $CD8^+$ TILs, and sorted $Sig9^-$ or $Sig9^+$ $CD8^+$ TILs (*n*=4-6). (**F**) Induction of apoptosis measured by cleaved caspase 3 (clCasp3) in HT-29 cells incubated with unsorted $CD8^+$ TILs, and sorted $Sig9^-$ or $Sig9^+$ $CD8^+$ TILs (*n*=4). (**G**) Inhibition of $CD8^+$ T cell activation by different anti-Siglec antibodies measured by flow cytometry. CD25 was determined on $CD8^+$ T cells stimulated by anti-CD3 and anti-CD28 antibodies in the presence of anti-Siglec-9 antibodies (191240, blocking IgG, E10-286, non-blocking IgG), anti-Siglec-5 antibody or LGALS3BP as ligand (*n*=6). (**H**) $Ki67^+$ $CD8^+$ T cells polyclonally stimulated in presence of antibodies (*n*=6). (**I**) $Ki67^+$ $CD8^+$ T cells polyclonally activated in presence of different concentrations of anti-Siglec-9 antibody (clone 191240 from R&D Biosciences, *n*=4). (**J**) Inhibition of binding of calcein AM-labeled A549 cells to immobilized Sig9-Fc in presence of clone 191240 antibody or isotype control (numbers represent $x10^3$ cells). **P*<0.05, ***P*<0.01, ****P*<0.001. Data presented as mean±s.d.

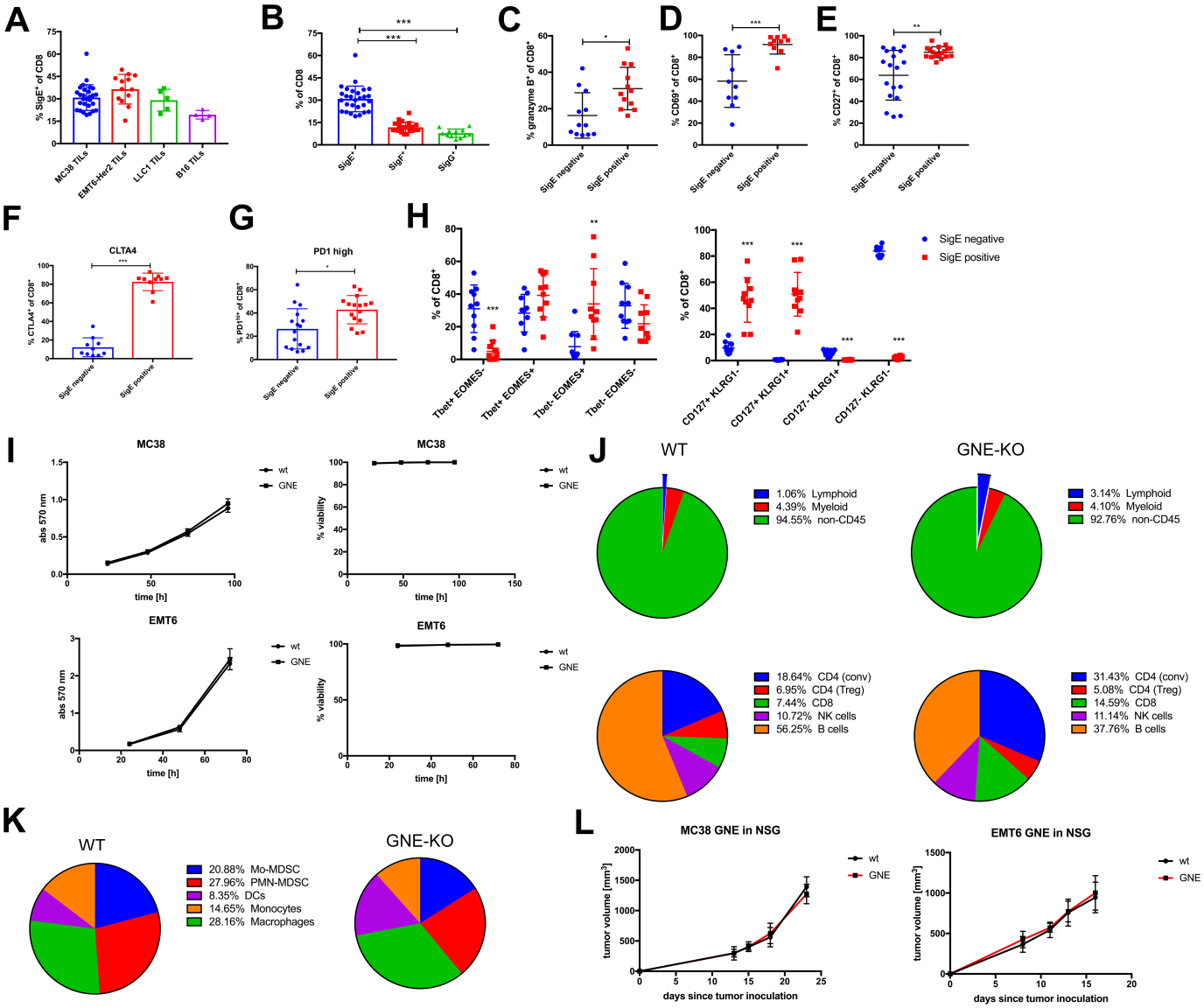

Supplemental Figure 8 Sialoglycan-SAMPs enhance tumor growth in vivo.

(**A**) Expression of Siglec-E in percent on CD8$^+$ TILs in different tumor models including MC38 (*n*=28), EMT6 (*n*=13), LLC1 (*n*=5), or B16 (*n*=4). All the analysis afterwards in this figure are from the MC38 model. (**B**) Expression of Siglec-E (n=28, same analysis as used in A), Siglec-F (*n*=21) or Siglec-G (*n*=12) on CD8$^+$ TILs in the MC38 subcutaneous tumor model determined by flow cytometry. (**C-E**) Expression of granzyme B (**C**, *n*=12), CD69 (**D**, *n*=10) and CD27 (**E**, *n*=18) on SigE$^-$ CD8$^+$ and SigE$^+$ CD8$^+$ TILs. (**F**) Percent of CTLA-4 expressing cells within the SigE$^-$ CD8$^+$ and SigE$^+$ CD8$^+$ TIL population (*n*=10). (**G**) Presence of PD^{hi} positive cells in the SigE$^-$ CD8$^+$ and SigE$^+$ CD8$^+$ TIL population (*n*=16). (**H**) Frequency of different EOMES and

Tbet expressing populations in the $SigE^{-}$ $CD8^{+}$ and $SigE^{+}$ $CD8^{+}$ TIL population (*n*=10). (**I**) Frequency of different CD127 and KLRG1 expressing populations in the $SigE^{-}$ $CD8^{+}$ and $SigE^{+}$ $CD8^{+}$ TIL population (*n*=10). (**I**) *In vitro* proliferation of GNE-KO MC38 and EMT6 cells compared to wildtype cells. The proliferation was assessed by an MTT assay. Viability of cells was measured by trypan blue exclusion. (**J, K**) Analysis of immune cell infiltrates by flow cytometry in subcutaneous MC38 tumors (*n*=7). (**L**) Subcutaneous tumor growth of MC38 GNE-KO or MC38 wildtype cells and EMT6 GNE-KO or EMT6 wildtype cells in NSG mice (*n*=6). **P*<0.05, ***P*<0.01, ****P*<0.001. Data presented as mean±s.d.

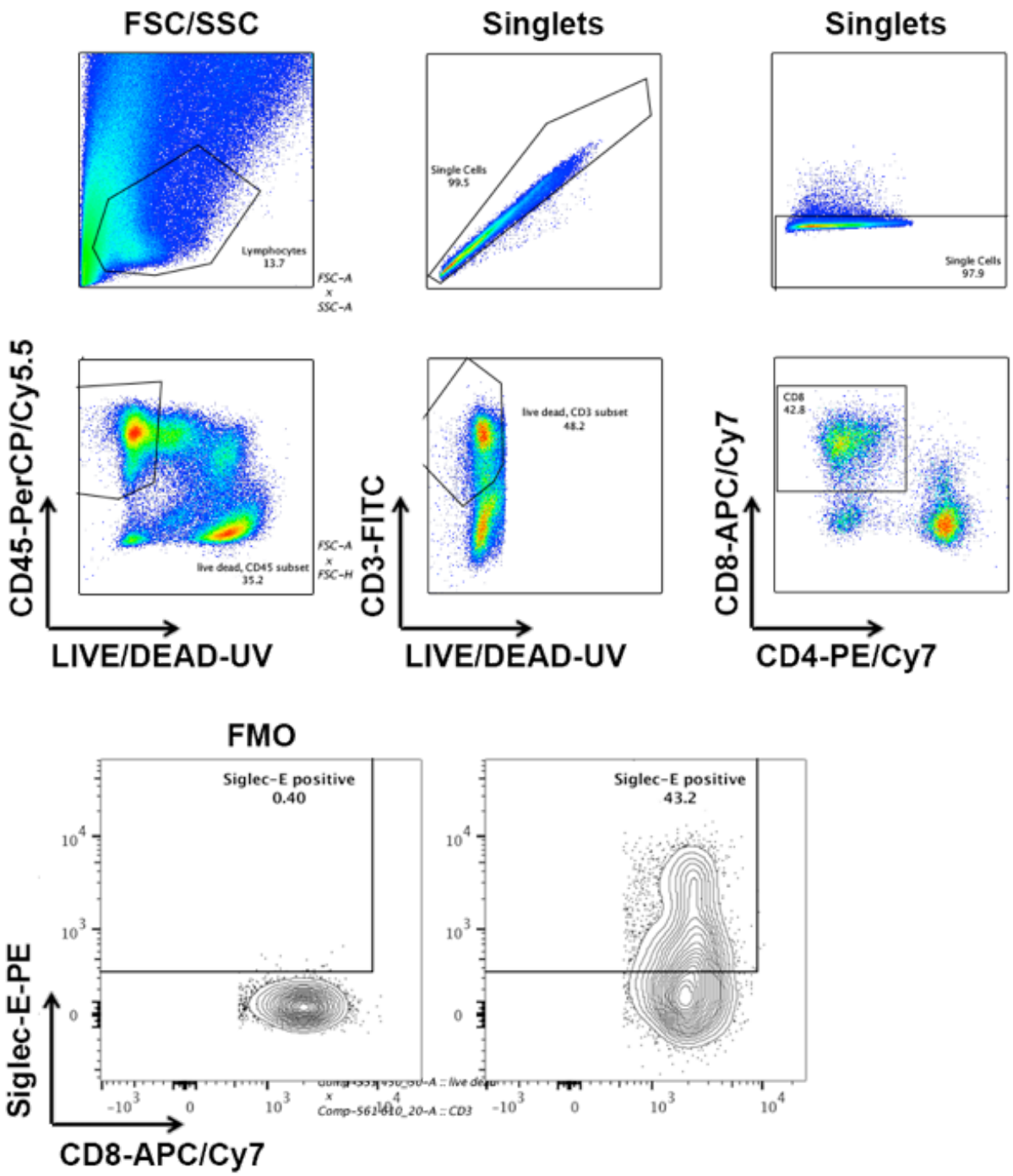

Supplemental Figure 9 Gating strategy for determination of Siglec-E expression on CD8$^+$ TILs.

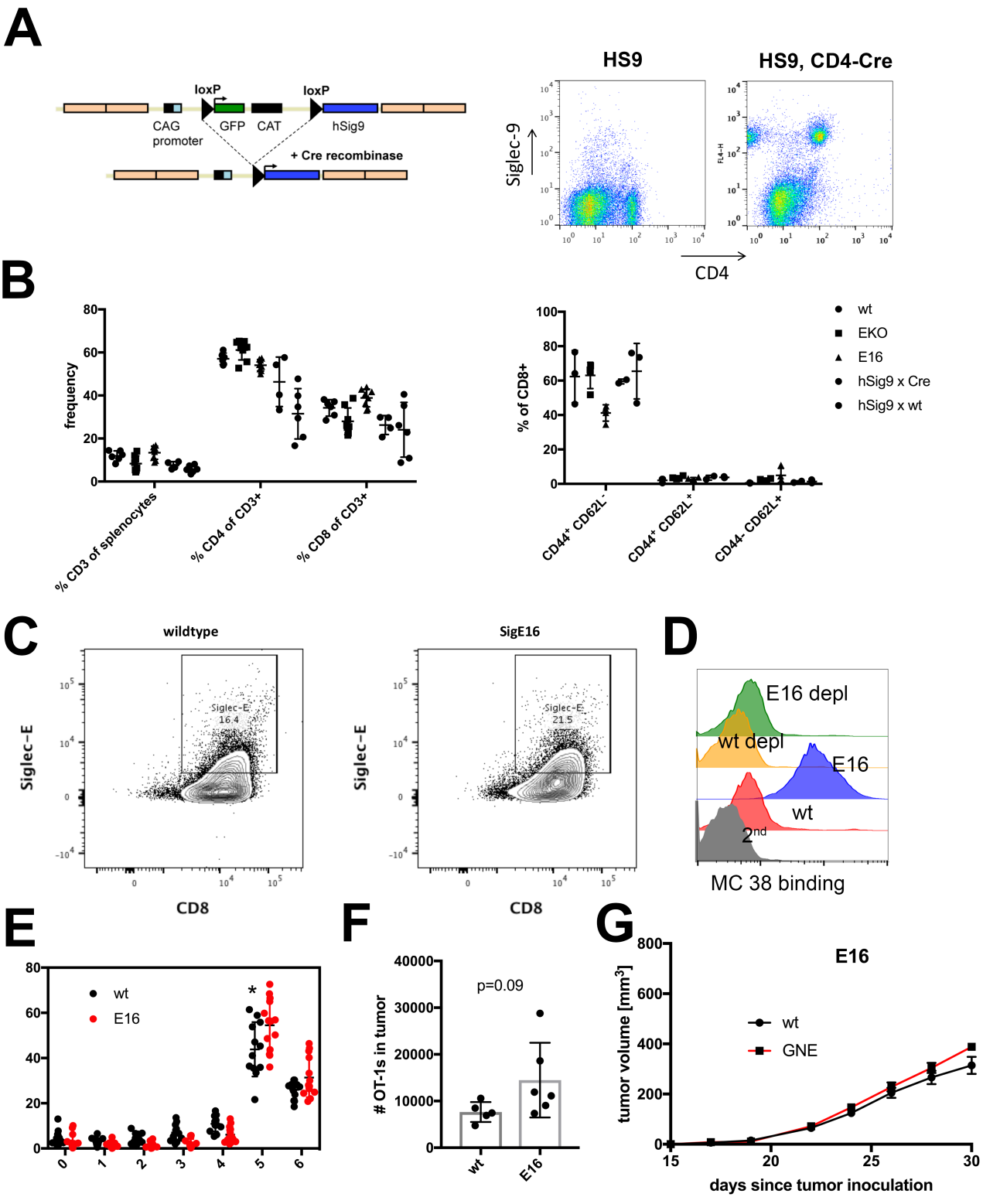
A
loxP
loxP
CAG promoter
GFP
CAT
hSig9
+ Cre recombinase
HS9
HS9, CD4-Cre
Siglec-9
CD4
B
frequency
% CD3 of splenocytes
% CD4 of CD3+
% CD8 of CD3+
% of CD8+
CD44+ CD62L-
CD44+ CD62L+
CD44- CD62L+
wt
EKO
E16
hSig9 x Cre
hSig9 x wt
C
wildtype
SigE16
Siglec-E
16.4
21.5
CD8
D
E16 depl
wt depl
E16
wt
2nd
MC 38 binding
E
wt
E16
*
F
p=0.09
# OT-1s in tumor
wt
E16
G
E16
wt
GNE
tumor volume [mm3]
days since tumor inoculation

Supplemental Figure 10 Genetic model for Siglec-9 expression in T cells.

(**A**) Schematic drawing of genetic rearrangement and flow cytometry analysis of splenocytes for Siglec-9 expression in HS9 mice and HS9 mice crossed to CD4-Cre mice (CD4-Cre HS9 mice). (**B**) Frequency of T cells and memory subsets in spleens from different genetic strains (*n*=4-6). (**C**) Frequency of Siglec expression on $CD8^+$ TILs in subcutaneous MC38 tumors. Representative FACS plots are shown. (**D**) Representative example of IgG binding of serum from different tumor-bearing mice to MC38 tumor cells. Binding was assessed by FACS analysis and secondary anti-mouse-IgG staining. (**E**) Proliferation measured by cell trace violet (CTV) of OT-1 T cells in MC38-OVA tumors after adoptive transfer. There is a higher frequency in the higher divisions (x axis, divisions, *n*=10). (**F**) Frequency of OT-1 T cells in MC38-OVA tumors after adoptive transfer (*n*=5-6). (**G**) Growth of GNE-KO MC38 wildtype MC38 cells in SigE16 mice (*n*=6). **P*<0.05. Data presented as mean±s.d.

Supplemental Table 1

rs2075803 alleles and odds ratio (OR) for CRC risk

	Control	Case	OR	*P* value
GG	935	1205		
AG	1469	1879	0.99 (0.88,1.11)	0.91
AA	640	711	0.86 (0.75,0.99)	0.04
Sum	3044	3795		

rs2258983 alleles and odds ratio (OR) for CRC risk

	Control	Case	OR	*P* value
AA	958	1237		
CA	1351	1730	0.99(0.89,1.11)	0.89
CC	546	573	0.81(0.70,0.94)	0.005
Sum	2855	3540		